Applied Clay Science 149 (2017) 20–27

Contents lists available at ScienceDirect

Applied Clay Science

journal homepage: www.elsevier.com/locate/clay

Research paper

Evaluation of polymeric Al-modified bentonite for its potential application as ceramic coating

J.M. Martinez*, C. Volzone, L.B. Garrido

CETMIC -Centro de Tecnología de Recursos Minerales y Cerámica- (CCT CONICET-La Plata; CICPBA), Camino Centenario y 506, CC49, M.B. Gonnet 1897, Buenos Aires, Argentina.

ARTICLE INFO

Keywords:
Bentonite
OH-Al polymers
Dip coating
Mullite

ABSTRACT

A polymeric Al-modified bentonite (B-OHAl) obtained by intercalation of OH-Al species was used as precursor for mullite-containing coatings. Raw clay and B-OHAl were characterized by X-ray fluorescence (XRF), Infrared spectroscopy (FTIR), X-ray diffraction (XRD), thermogravimetric and differential thermal analysis (TG-DTA). Rheological and electrokinetic behavior of B-OHAl dispersions were optimized by the addition of sodium polyacrylate (NaPA) for its use in dip coating on ceramic substrates. Moderate densification and mullite development of B-OHAl by thermal treatment up to 1200 °C was observed by mercury intrusion porosimetry (MIP), XRD and scanning electron microscopy SEM. NaPA addition on dispersions and an increase in porosity values in substrate led to higher amounts of coating retained in dip coated composites sintered at 1200 °C.

1. Introduction

Ceramic coatings are commonly used in industry, as they can develop interesting properties, such as good corrosion and wear resistance, hardness, high temperature-strength, and thermal stability. These materials have a wide array of applications, as hard coatings for cutting tools (Bobzin, 2016), nuclear fuel cladding (Alat et al., 2016), antibacterial coating (Lee et al., 2016) and as thermal barriers (Bernard et al., 2016), among others.

Mechanical properties of ceramics are linked to the presence of certain crystalline phases. Being the only stable intermediate phase in the Al_2O_3–SiO_2 system at atmospheric pressure, mullite ($3Al_2O_3 \cdot 2SiO_2$ theoretical composition, with 72 mass% alumina and 28 mass% silica) is one of the most important ceramic materials, due to its refractory nature, good chemical stability, high-temperature strength, low thermal conductivity and expansion coefficient (Duval et al., 2008). Mullite is usually synthesized, as it is rarely found in nature. Anggono (2005) reported that there are mainly three synthesis methods for mullite. The more classical method involves the mixture of clays (kaolin) and other aluminum containing materials, which, upon sintering, form mullite. Another method involves the melting of the raw materials (for example, alumina and sand) in furnace at temperatures above 2000 °C. The third method is the so-called "chemical-mullite" synthesis, which involves the mixing of Al^{3+} and Si^{4+} on scales ranging from the atomic to the micron level. This method has the advantage of being able to reduce the sintering temperature to lower values than with mixed solids.

The interlayering of smectites with inorganic polycationic species has been widely studied, as these materials form Pillared Interlayer Clays (PILC) when thermally treated at 350 °C–750 °C (Brindley and Sempels, 1977; Vaughan and Lussier, 1980; Vicente et al., 2001; Aouad et al., 2005). PILC have seen widespread application in various fields such as the production of biofuels (Kloprogge et al., 2005), catalysis (Kanda et al., 2009), adsorption of heavy metals (Bhattacharyya and Gupta, 2008) among others; due to their high surface area and thermal stability (Kloprogge, 1998). Also, the intercalating polycation $[Al_{13}O_4(OH)_{24}(H_2O)_{12}]^{7+}$, usually known as Al_{13} cation, is simple to synthesize reproducibly (Wang et al., 2016). One interesting feature of these Al-interlayered clays, which has been scarcely studied, is that they can develop mullite when thermally treated. Martinez et al. (2017) used two montmorillonitic clays, namely a Wyoming and a Cheto one (both samples from USA) to obtain Al-interlayered clays, and found mullite presence after thermal treatment above 1000 °C. Jagota et al. (1995) studied an Al-interlayered smectite and found evidence of mullite formation at 800 °C, which is a relatively low temperature.

At temperatures above 800 °C, the Al-interlayered clays lose their characteristic layered structure as their interlayer space collapses (Kloprogge et al., 1994; Vicente et al., 2001; Volzone and Garrido, 2012). At higher temperatures, they develop stable crystalline phases (Jagota et al., 1995; Martinez et al., 2017). Due to their natural origin, the formation of crystalline and liquid phases at high temperature in clays is conditioned by several factors, such as the chemical and mineralogical composition of the clay mineral, the presence of structural

* Corresponding author.
E-mail address: juanmartinez@cetmic.unlp.edu.ar (J.M. Martinez).

http://dx.doi.org/10.1016/j.clay.2017.09.004
Received 8 March 2017; Received in revised form 15 August 2017; Accepted 4 September 2017

defects and impurities, etc. (McConville and Lee, 2005; Martinez et al., 2017). Consequently, the microstructure and properties of the fired Al-intercalated clay mineral greatly differs from those of the untreated (fired) one.

There are many ways of producing mullite-containing coating on substrates. Plasma spraying (Schrijnemakers et al., 2009), sol-gel (Zhongliu et al., 2015), hot dipping (Zhang et al., 2016), electrophoretic deposition (Wang et al., 2013), and dip coating (Ramasamy et al., 2011) among others. Dip coating is a simple, inexpensive method of depositing uniform thin layers of particles in dispersion onto a substrate which, upon evaporation of the liquid, forms a film of coating. The film thickness is set by the competition among viscous force, capillary force and gravity (Scriven, 1988). Thus, a basic requirement for the application of this method is the preparation of stable and fluid dispersions. To achieve these characteristics, the understanding of the dispersion of the particles in a liquid medium is of paramount importance. Viscosity of aqueous dispersions can be modified by the addition of different chemical agents.

Although rheological properties of bentonite dispersions and the influence of the addition of dispersants were extensively investigated (Lagaly, 2006; Liang et al., 2010; Santagata et al., 2014), there are limited studies available on colloidal, electrokinetic and rheological properties of Al-intercalated smectite dispersions (Harsh et al., 1988; Avena et al., 1990). Jagota et al. (1995) used Al-intercalated smectite dispersions to coat SiC fibers which, upon firing, were included in a borosilicate glass matrix, improving its mechanical properties; though no rheological properties of the dispersions were measured. The measurement and control of these properties are essential for the preparation of stable dispersions in order to produce dip-coated composites.

The objective of this work was to study the properties of a polymeric Al-modified bentonite (B-OHAl) in order to evaluate its possible application as a precursor for mullite-containing coatings on ceramic substrates. Crystalline phases and textural properties developed in B-OHAl through thermal treatment at high temperatures (1000–1200 °C) were determined by powder X-ray diffraction (XRD), infrared spectroscopy (FTIR) and mercury intrusion porosimetry (MIP), respectively. Stability of B-OHAl aqueous dispersions for dip coating and its modification by sodium polyacrylate addition was also examined by electrophoretic mobility and viscosity measurements. Coated composites were obtained by dip coating a porous substrate in stable and unstable B-OHAl dispersions. Mullite formation and microstructure of coated surfaces was observed by XRD and scanning electron microscopy (SEM) respectively.

2. Experimental

2.1. Materials and methods

2.1.1. B-OHAl preparation

A bentonite from Argentina (B), with 15.6 mass% Al_2O_3 content was used to prepare the coating precursor. This bentonite has been characterized in a previous work (Vidal and Volzone, 2012) and is composed mainly by montmorillonite with traces of quartz and feldspar. The calculated structural formulae of the montmorillonite is: $[(Si_{3,94}Al^{IV}_{0,06})(Al^{VI}_{1,36}Fe_{0,06}Mg_{0,60})O_{10}(OH)_2]$.

Swelling index was obtained by adding 2.0 g of bentonite in a 100 ml measuring cylinder with water. After 24 h the height of sediment in ml was read. The swelling index of B was 4 ml. This value is low compared with an expansive bentonite, which reaches value > 12 ml.

The polymeric Al-modified bentonite (B-OHAl) preparation method has been previously reported (Volzone and Garrido, 2008), therefore, only a brief summary is described in this work. A polymeric hydroxyl-Al solution (0.10 M in Al) was prepared by diluting the commercial chlorohydroxy-Al solution (6.0 M) that was aged during 7 days at room temperature. The raw clay was dispersed in water (2 mass%) and subsequently the polymeric solution OH-Al was added. The aluminum/raw clay ratio was 3.25 mmol/g. After 24 h, the solid was separated by centrifugation and washed several times with distilled water in order to remove excess electrolyte.

In order to study of the influence of the heating temperature on the textural properties of B-OHAl, cylindrical casted samples were made by consolidation of the B-OHAl dispersion without additives. Slip casting of this dispersion was carried out in a plaster mould, obtaining samples of about 10 mm in diameter and 8–10 mm of thickness. The resultant cast cylinders were dried at room temperature for 24 h.

Both powdered samples and B-OHAl compacts were thermally treated in an electric furnace at a heating rate of 5 °C min^{-1} up to 1000, 1100, 1200 °C for 1 h.

2.1.2. Preparation of dip-coated composites

In order to obtain substrates with different porosity for dip coating, disk-shaped ceramics (diameter = 20 mm, thickness = 5 mm) were prepared using a commercial clay by uniaxial compression of the powder at 30 MPa and subsequent thermal treatment at 800 °C (S800) and 1100 °C (S1100) in an electric furnace. The commercial clay is mainly composed by quartz, kaolinite, illite and feldspar. Substrate showed an open porosity of 32.1% and a mean pore diameter of 65.3 nm when thermally treated at 800 °C for 1 h and an open porosity of 18.1% and a mean pore diameter of 330 nm after firing at 1100 °C for 1 h.

Aqueous dispersions of B-OHAl with and without the addition of sodium polyacrylate (NaPA, Dolapix PC 67, Zschimmer & Schwarz) were used as coating precursor. They were obtained by dispersing 6 g of B-OHAl in 100 ml of distilled water containing the dispersant up to desired concentration and stirred for 1 h at room temperature.

Preliminary dip-coating tests were made in order to evaluate the influence of dip coating time (5, 10, 20 and 40 s) on the amount of coating retained. It was observed that the latter increased with coating time up to 10 s, while for longer times it remained relatively constant but favored cracking of the coating surface. Thus, dip-coated composites were obtained by dipping the calcined substrate disks in these dispersions for 10 s, and left to dry at room temperature until constant mass. This process was repeated 3 times. The dip-coated substrates were dried overnight at room temperature and then 1 h at 60 °C in an electric oven prior to thermal treatment, which was carried out in an electric furnace at a heating rate of 5 °C min^{-1} up to 1200 °C for 1 h. The adherence of the fired coating was evaluated by pushing a scotch tape onto the coated surface and then pulling fast. This test made it possible to establish that the coating adhered firmly to the substrate after doing so.

2.2. Characterization techniques

Chemical analysis of samples was done by X-ray fluorescence (XRF, Shimadzu EDX800-HD). The identification of crystalline phases and structural characterization of raw clay, B-OHAl and the thermally treated samples was carried out by X-ray diffraction (XRD), using a diffractometer Philips with goniometer 3020 and PW3710 controller with radiation of Cu-Kα and Ni filter in the range of 3–70°(2θ). FTIR analysis of B and B-OHAl samples were performed by using a Spectrum One Perkin Elmer equipment, in the wavelength range of 400–4000 cm^{-1}. The samples were dispersed in KBr (1 mass%) and compacted in a thin pellet form.

Thermogravimetric and differential thermal analysis (TG-DTA) of samples up to 1200 °C was performed with a Netzsch 409 equipment, using α-Al_2O_3 as reference at a heating rate of 10 °C min^{-1}.

Electrophoretic mobility measurements at different pH were made. Powdered sample (< 144 μm) was dispersed in a 500 ml KCl solution (10^{-3} M) to 0.1 mass% solid concentration. The pH of the dispersions was adjusted by addition of 0.01 M NaOH or 0.01 M HCl. Electrophoretic mobility measurements were carried out using a ZETA PLUS zeta potential analyser (Brookhaven Instruments, USA).

Electrophoretic mobility of the B-OHAl dispersion containing sodium polyacrylate (NaPA, Dolapix PC 67, Zschimmer & Schwarz) at different pH was also determined.

The effect of the addition of NaPA in a 0–4.2 NaPA/B-OHAl (% g/g) ratio on the flow curves (i.e. the shear stress vs. strain rate) and bulk viscosity of the dispersions was measured. Rheological measurements of aqueous B-OHAl dispersions (40 mass%) were performed with a rotational viscometer (Haake VT 550) at 25 °C. Flow curve of the dispersion was determined by linearly increasing the shear rate up to a maximum of 550 s^{-1} and then decreasing, point by point, in stationary conditions.

Open porosity and bulk density measurements of B-OHAl compacts and substrate were performed using mercury intrusion porosimetry (MIP). The equipment used was an automatic porosimeter (Pascal 440, Thermo Fisher Scientific Inc.)

Amount of coating in each composite (mg cm^{-2}) was calculated based on the mass of the substrate before and after coating (and thermal treatment) in an analytical balance. The microstructure of the surface of both coated composites and uncoated substrates (sintered at 1200 °C) was observed with a scanning electron microscope (SEM, JCM-6000, JEOL).

3. Results and discussion

3.1. Characterization of B-OHAl as coating precursor

X-ray fluorescence (XRF) chemical analyses of natural and polymeric Al-modified bentonite (Table 1) showed that the Al_2O_3/SiO_2 ratio increased from 0.3 g/g in B to 0.5 g/g in B-OHAl, thus indicating that aluminum was incorporated by the OH-Al species in the treated clay. Simultaneous reduction of the interlayer cations content (i.e., Ca^{2+} and Na^{+}) after OH-Al species retention was also observed, suggesting that the OH-Al species have displaced interlayer cations in the clay mineral (Kloprogge, 1998; De León et al., 2014). Previous works (Volzone and Garrido, 2001; De León et al., 2014) have shown that the OH-Al species present in the precursor solution used for the intercalation of the clay mineral contain mainly Al_{13} polymeric species $[Al_{13}O_4(OH)_{24}{\cdot}12H_2O]^{7+}$, which would explain the LOI increase after treatment, as such species contain a high amount of OH^-.

Infrared spectra of bentonite B (Fig. 1) shows bands typical of montmorillonite at 3640, 3441, 1102,1026, 913, 837, 520, 465 cm^{-1} and a band at 794 cm^{-1} which corresponds to small amounts of quartz. The bands at 3640 and 3441 cm^{-1} are respectively assigned to OH-stretching vibration (Al—Al—OH) and OH^- from intercalated water in the montmorillonite. The band at 1640 cm^{-1} is attributed to OH vibration bending of H—O—H. The Si—O—Si stretching parallel and perpendicular vibrations bands are at 1026 and at 1102 cm^{-1}, respectively. The bands at 913 and 837 cm^{-1} are respectively assigned to the bending vibrations of Al—Al—OH and Mg—Al—OH groups. The bands at 510 and 465 cm^{-1} correspond to Si—O—Al^{IV} and Si—O—Si structural groups of the clay mineral (Farmer, 1968). The OH-stretching vibration absorption band of montmorillonite at 3640 cm^{-1} were shifted to slightly lower wavenumbers, 3629 after intercalation of OH-Al species in the montmorillonite clays. Therefore, the OH group of the OH-Al species might be contributing to the OH-stretching band with more energy than that of the clay structure. The bands near 1026 cm^{-1}, 913 cm^{-1} and 837 cm^{-1} of the smectite assigned to the Si—O bond, Al—OH and Mg, Al—OH groups, respectively, shifted to slightly higher wavenumbers 1029–1087, 915 and 847 cm^{-1} in intercalated OH-Al montmorillonite, maybe attributed to the changes in the structure clay minerals due to the intercalation process (Volzone and Garrido, 2001).

Table 1
Chemical composition of B and B-OHAl (mass %).

	SiO_2	Al_2O_3	Fe_2O_3	CaO	MgO	Na_2O	K_2O	TiO_2	LOI
B	51.30	15.60	1.20	1.21	5.18	2.62	0.63	0.23	20.80
B-OHAl	43.20	22.00	1.07	0.42	4.38	0.43	0.46	0.20	26.00

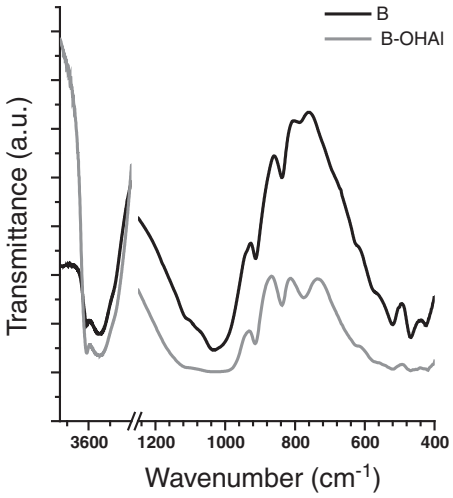

Fig. 1. FTIR spectra of B and B-OHAl samples.

Montmorillonite reflections in the XRD of the bentonite after OH-Al treatment (B-OHAl) were found accompanied with quartz and feldspar in scarce amounts as impurities (Fig. 2a). The d-value shifted from 14.8 Å in B to 19.0 Å in B-OHAl (Fig. 2b) due to the intercalation of the OH-Al species in montmorillonite. This value corresponds to a calculated interlayer space of ≈ 9.4 Å, in B-OHAl (i.e. basal spacing minus the thickness of the layer of clay mineral 9.6 Å), which is close to the size of Keggin-like $(Al_{13}O_4(OH)_{24}(H_2O)_{12})^{7+}$ cations (≈ 9.0 Å) (Vaughan and Lussier, 1980; Plee et al., 1985; Ma et al., 2015), indicating that these OH-Al polymeric species were located in the interlayer space (Volzone and Garrido, 2001).

DTA of the raw bentonite (Fig. 3a) shows a typical thermal curve of montmorillonite, with two endothermic peaks at around 100 °C and 600 °C, indicating the dehydration and dehydroxylation of the clay mineral structure respectively. The S-shaped *endo*-exothermic peaks at higher temperature (800–850 °C) are associated to the collapse of the clay mineral structure and the appearance of new crystalline phases (Mackenzie and Caillère, 1979).

The intercalation of OH-Al species originated important changes in

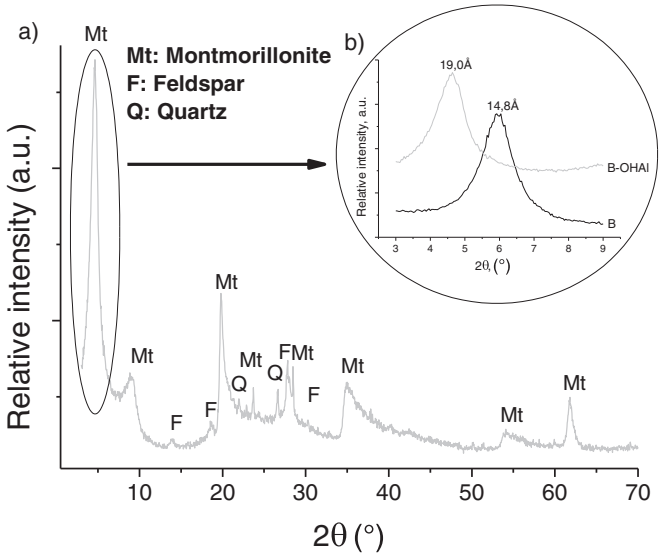

Fig. 2. X-ray diffraction patterns of a) B-OHAl b) comparative d_{001}-value of B and B-OHAl.

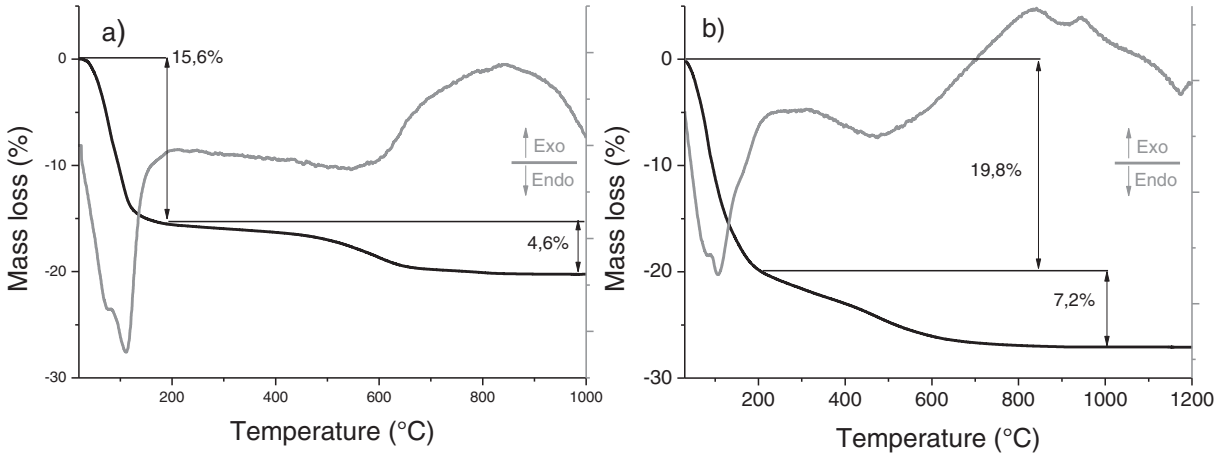

Fig. 3. DTA-TG curves of a) B and b) B-OHAl.

the DTA curve of B-OHAl (Fig. 3b). The first endothermic peak broadened slightly, while the second shifted to lower temperatures (480 °C). These changes in thermal behavior are associated to the forming of chemical bonds between OH-Al species and the montmorillonite layers (Aceman et al., 2000; Volzone and Garrido, 2001). The S-shaped peak of B-OHAl was centered at higher temperatures (880–950 °C).

TG curve of B showed a mass loss of 15.6% up to 200 °C, attributed to the loss of adsorbed water and the hydration water of the interlayer cations (Mackenzie and Caillère, 1979). The mass loss of B-OHAl up to 200 °C was 19.8%, being this higher value related with the intercalated OH-Al species (Volzone and Garrido, 2001; De León et al., 2014). As mentioned before, the interlayered OH-Al species are mainly poly-nuclear-Al_{13} cation. The dehydration-dehydroxilation of these species with heat treatment is reflected in these higher values of mass loss for the precursor.

The removal of structural hydroxyls of the montmorillonite (mass loss of 4.6%) occurred in a relatively narrow range (500–700 °C), while the removal of those hydroxyls in the precursor was more gradual, in a wider range of temperatures (200–700 °C). No significant mass changes above 800 °C were observed in either sample. The total mass loss up to 1000 °C for B and B-OHAl were 20.0 and 27.0 mass% respectively, mainly attributed to the presence of OH-Al species in the interlayer spacing of the montmorillonite.

The effect of thermal treatment on phase development and textural properties of B-OHAl as coating precursor was determined. For comparison, in the XRD patterns of B clay (Fig. 4a) no montmorillonite reflections were observed at 1000 °C due to the collapse of the clay mineral structure (Grim, 1961; Mackenzie and Caillère, 1979) and other crystalline phases were found. Magnesium aluminosilicate ($(Mg,Al)SiO_3$) and spinel ($MgAl_2O_4$) were developed, and minor amounts of unreacted feldspar (anorthite - $(Ca,Na)(Al,Si)2Si_2O_8$) and quartz (SiO_2) were present. At 1100 °C, spinel reflections became more intense, and cristobalite (SiO_2) appeared, while feldspar reflections began to decrease in intensity. At 1200 °C, feldspar reflections disappeared, cristobalite remained while sapphirine ($(Al_5Mg_4)(Al_4Si_2)O_{20}$) and cordierite ($Mg_2Al_4Si_5O_{18}$) reflections were observed. It is important to note that, for all analyzed samples, a broad band centered at around ~ 22°2θ was observed, associated to the presence of an amorphous phase (Gavin et al., 2013). At thermal treatment above 800–900 °C, a silica-rich liquid phase is formed due to the melting of the silica tetrahedral of the montmorillonite sheet and alkalis present which, upon cooling, forms this vitreous (amorphous) phase (McConville and Lee, 2005; Lee et al., 2008). Aluminum content on the montmorillonite clay structure was not enough for it to develop mullite after thermal treatment up to 1200 °C. Instead, the presence of structural Mg favored the development of cordierite.

In the XRD diffractograms of the thermally treated B-OHAl sample (Fig. 4b), magnesium aluminosilicate reflections could not be observed at 1000 °C. This could be attributed to the presence of higher amounts of aluminum than the raw clay, as observed in previous works (Martinez et al., 2017). Spinel reflections were also observed, and reflections of quartz and feldspar were present, with an important amorphous phase contribution. At 1100 °C, reflections corresponding to mullite ($3Al_2O_3 \cdot 2SiO_2$) and those of cristobalite significantly grew,

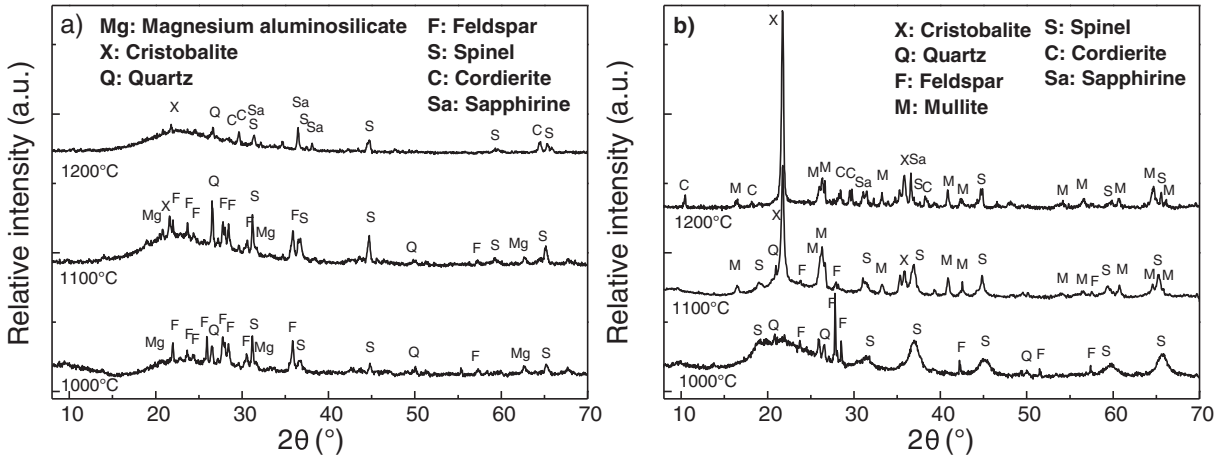

Fig. 4. XRD plot of a) B and b) B-OHAl thermally treated at different temperatures.

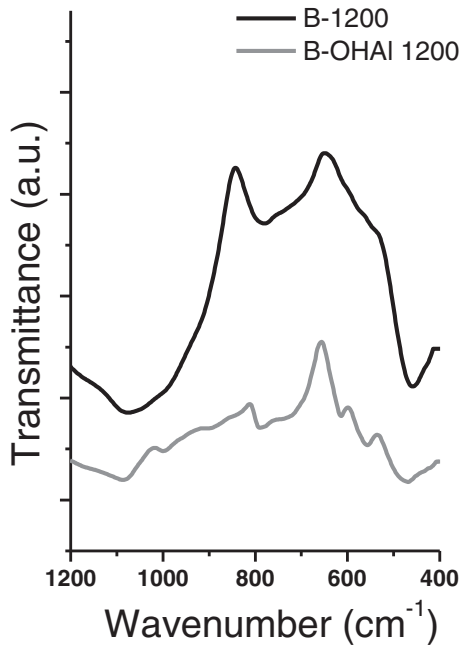

Fig. 5. FTIR spectra of B and B-OHAl samples heated at 1200 °C.

while the "hump" at ~ 22°2θ reduced in intensity, indicating a lower amorphous phase content. Mullite development in polymeric Al-modified clays has been previously studied, and is associated to the higher Al/Si ratio and the "mixture" of Al^{3+} and Si^{4+} on atomic scales; i.e.: the interlayering of Al-polymeric species in the clay mineral layers (Jagota et al., 1995; Volzone and Garrido, 2012; Martinez et al., 2017). At 1200 °C mullite reflections increased in intensity, while spinel reflections reduced. Feldspar reflections disappeared, cordierite appeared and the amount of amorphous phase reduced drastically. The additional aluminum in the Al-intercalated clay contributed to the development of mullite after thermal treatment. It also contributed to a more crystalline structure at temperatures above 1100 °C (i.e.: less amorphous content) compared to the untreated bentonite.

A comparative infrared analysis between B and B-OHAl after thermal treatment at 1200 °C (Fig. 5) evidenced the formation of the mullite in B-OHAl-1200 due to presence of main bands at 557, 620, 740, 850 cm^{-1} corresponding to bending Al—O (AlO_6), bending O—Al—O (AlO_4); bending Al—O (AlO_4), stretching Al—O(AlO_4), respectively. (Dietmar et al., 2001).

Open porosity and bulk density of B-OHAl compacts changed with thermal treatment at different temperatures (Table 2). Increasing temperature resulted in an increase in bulk density, accompanied with a decrease in open porosity. Open porosity remained approximately constant (~ 20%) between 1100 °C and 1200 °C, indicating a relatively higher thermal stability of B-OHAl sample than that of B, which showed a higher amorphous phase content at this temperature (Fig. 4). This may be attributed to the OH-Al species interlayered, which enhanced the formation of mullite and other crystalline phases and reduced the content vitreous phase. A reduction of open porosity in ceramics is

Table 2
Open porosity and bulk density of B-OHAl compacts thermally treated at different temperatures.

Temperature of thermal treatment (°C)	Bulk density (g cm^{-3})	Open porosity (%)
1000	1.79	36.0
1100	1.90	20.2
1200	2.18	19.9

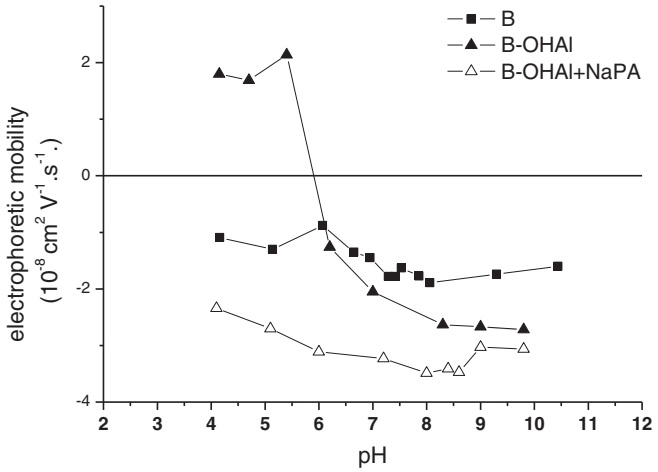

Fig. 6. Electrophoretic mobility of dispersions of B, B-OHAl and B-OHAl with NaPA addition.

usually associated with an increase in mechanical properties, such elastic moduli and strength (Wachtman et al., 2009).

3.2. Dispersion and flow properties of B-OHAl aqueous dispersions

Electrophoretic mobility values of raw clay particles (Fig. 6) were negative in the range of pH studied (4–10.5), and its magnitude slightly increased from -1 to $-1.5 \times 10^{-8}\ cm^2(V.s)^{-1}$ with increasing pH. Thus, the particles have a net permanent negative charge as expected for these types of clays in agreement with results previously reported (Avena et al., 1990; Lagaly, 2006). The permanent negative charge is the consequence of the high degree of isomorphic substitution in the clay mineral present in the bentonite (see structural formulae). Some Al^{3+} ions in the octahedral sheet are substituted by Fe^{2+} and Mg^{2+} in addition to some substitution of Si^{4+} of the tetrahedral layer by Al^{3+}. At more alkaline pH values, the net negative surface charge slightly increased, mainly due to the progressive neutralization of silanol and Al-OH_2^+ groups on exposed sites of the edge surface of the clay mineral particles.

B-OHAl dispersion showed positive electrophoretic mobility values up to pH ~ 6, where the curve abruptly changed to negative values, indicating an isoelectric point at pH ~ 6 (pH iep). This indicates that the surface charge developed by B-OHAl particles remained positive between pH 4 and 6 due to the contribution of positive charge of intercalated OH-Al species in acidic medium, largely compensating the net negative charge. This behavior of polymeric Al-modified montmorillonite dispersions was previously observed in other works (Bottero et al., 1988) and is attributed to the OH-Al polymeric species intercalated in the clay mineral.

Thus, the difference in electrophoretic mobility between B-OHAl and the raw clay was higher at lower pH values, and reduced with increasing pH. This is because of the charge of the OH-Al polymeric species is opposite to that of the clay in acidic media and reverses with the pH of the dispersion. The OH-Al groups which are constituents of the Al species are amphoteric, and due to association and dissociation of H^+, their positive charge is neutralized with increasing pH, becoming negative at alkaline pH values. Therefore, its negative charge helped to increase the magnitude of the negative mobility in alkaline medium compared with that of B clay particles (Avena et al., 1990).

The effect of NaPA addition in a 2.8 NaPA/B-OHAl %g/g ratio on electrophoretic mobility of B-OHAl dispersions was also analyzed (Fig. 6). Between pH 4.5 to about 12 NaPA molecules are fully ionized, thus enabling the electrostatic interaction between their negative charge and the particles in the dispersion (Mathieu et al., 2008). For B-OHAl dispersion containing NaPA, negative electrophoretic mobility

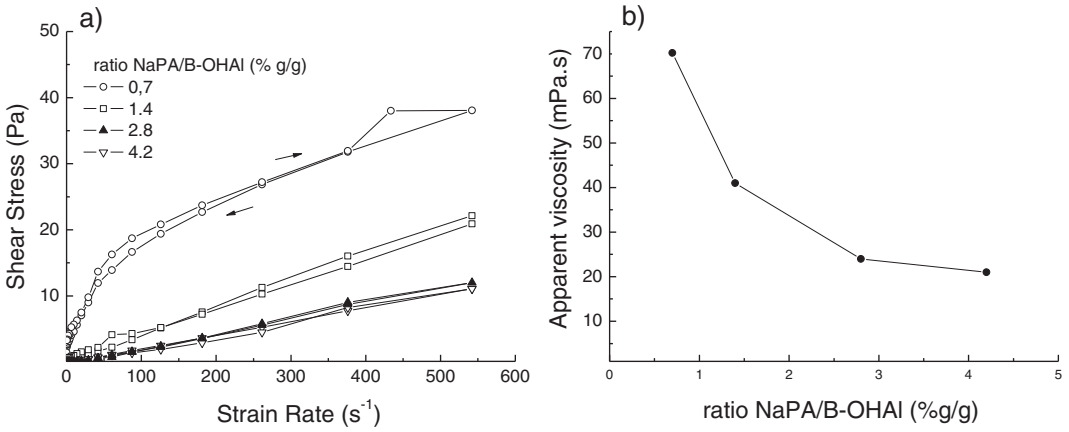

Fig. 7. a) Flow curves and b) apparent viscosity of B-OHAl dispersions (40% g B-OHAl/g dispersion) vs. NaPA concentration.

values were found in the pH range studied. Until pH ~ 8.4, the curve can be explained by the specific adsorption of R—COO^- groups of NaPA with the interlayered OH-Al polycations, which favored the electrostatic repulsion between the particles. Although adsorption of NaPA molecules onto the clay mineral layers is expected to be relatively low on montmorillonites (Siffert and Espinasse, 1980), NaPA molecules were found to electrostatically interact with positively charged OH-Al species (Mathieu et al., 2008; Choon Ong Ban, 2010) providing increasing colloidal stability, i.e.; higher negative electrophoretic mobility and zeta potential values. The slight reduction in negative electrophoretic mobility of particles with PA adsorbed at pH > 8 may be explained by the decrease in adsorption caused by an increase in electrostatic repulsion between the COO − group from the ionized NaPA molecules and negatively charged sites on B-OHAl surface (Siffert and Espinasse, 1980). The relative amount of negative sites on B-OHAl particles increased with increasing pH above the isoelectric point as indicated by electrophoretic mobility measurements.

The flow properties of 40 mass% aqueous dispersions of B-OHAl containing NaPA were measured (Fig. 7a). As dispersions prepared without NaPA exhibited high consistency due to the flocculation of particles, their rheological measurements could not be performed.

Dispersions with a NaPA/B-OHAl ratio of 0.7%g/g exhibited relatively high shear stress values (i.e. high apparent viscosity) and a pseudoplastic /shear thinning flow behavior in which apparent viscosity decreased with increasing shear rate. With increasing NaPA addition up to a 1.4 NaPA/B-OHAl %g/g ratio, the flow behavior became newtonian (linear relation between shear rate and shear stress indicating a constant viscosity) and the dispersion exhibited a significant decrease in shear stress values.

The dispersions with higher NaPA concentrations (2.8 and 4.2 NaPA/B-OHAl %g/g) maintained the newtonian behavior and attained lower viscosities than those with a lower NaPA concentration. A marked reduction in viscosity was observed up to 2.8 NaPA/B-OHAl % g/g (Fig. 7b), whereas viscosity reached a plateau for further additions of NaPA. Thus, NaPA addition up to a 2.8 NaPA/B-OHAl %g/g ratio was the optimum required to obtain a minimum in viscosity of 22 m Pa·s, which may be indicative of a well stabilized dispersion.

Addition of NaPA caused significant changes in the electrophoretic mobility of B-OHAl particles (Fig. 6). The particles did not exhibit an isoelectric point and remained negatively charged in the pH range studied. Adsorption of polyacrylate on the B-OHAl surface enhanced negative electrophoretic mobility in comparison with the sample without dispersant, even in the alkaline pH medium. This resulted in a high electrostatic repulsion between particles and additionally the steric repulsion of the adsorbed polyacrylate layer probably contributed to enhance the stabilization of B-OHAl dispersion.

Thus, the improvement in the degree of dispersion and the reduction in viscosity of B-OHAl dispersion (Fig. 7b) may be explained by electrosteric stabilization mechanism provided by the sodium polyacrylate adsorption.

3.3. Coating of ceramic substrates and characterization of coated composites

B-OHAl dispersions (6 mass%) with and without NaPA addition were prepared to study the effect of the dispersion condition on microstructural properties of the coated composites obtained from the different porous substrates calcined at 800 and 1100 °C. Coated amount of B-OHAl on each substrate was expressed as retained mass per unit area (mg cm^{-2}), for different dispersions used (Fig. 8). The mass of the coating depended on the textural characteristics of the substrates. Composites obtained from the more porous substrate S800 resulted in greater retained amounts of coating, regardless of the precursor dispersion used. This result can be attributed to the higher capillary suction developed by the high volume of smaller pores (68 nm–32.1%) in the S800 substrate in comparison with the less porous one, S1100 (330 nm–18.1%). Capillary suction helps the formation of a layer of particles on external surface of the substrate by dip coating, as the liquid is absorbed into the pores (Scriven, 1988; Bouwmeester et al., 1996; Gu and Meng, 1999), which, upon firing, ultimately led to higher amounts of B-OHAl retained in this coated composite.

As mentioned before, NaPA addition to the B-OHAl dispersion avoided flocculation of particles, thus enabling the preparation of well stabilized dispersions. It also led to higher amounts of coating retained

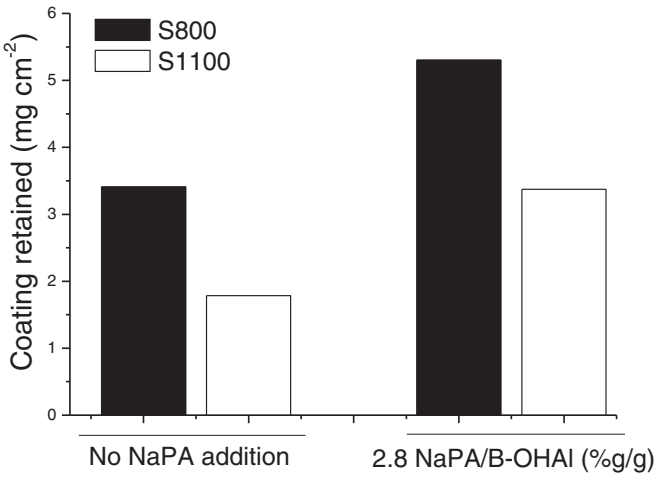

Fig. 8. Amount of coating retained (mg cm^{-2}) in dip-coated composites with different substrates and precursor dispersions.

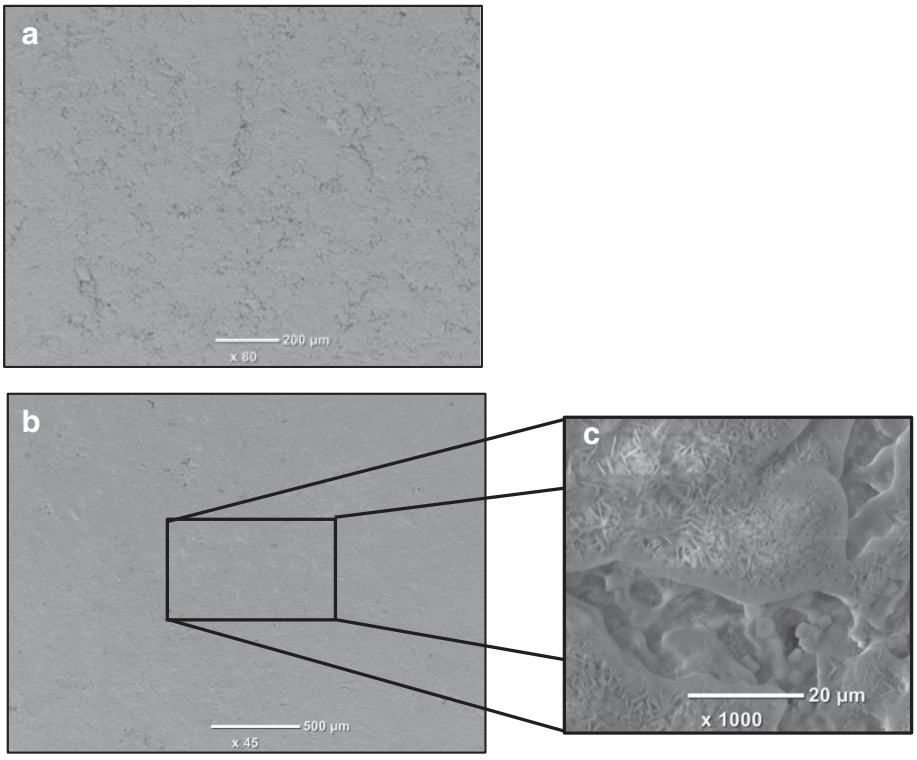

Fig. 9. SEM images of a) Substrate b) Coated composite thermally treated at 1200 °C. Etched coated composite images (c) reveal its microstructure in further detail.

for composites prepared by dipping in the stable dispersion in comparison with those obtained from the dispersion without additives.

Textural differences between uncoated substrate and coated composites sintered at 1200 °C can be observed (Fig. 9a and b). Although the coating appeared well adhered to the substrate, shrinkage during thermal treatment led to some cracking of the coating.

Cracking of coated composites is usually observed, and different approaches to solve this problem have been previously reported. Xia et al. (2000) studied the influence of successive dipping (i.e. dip coating, drying and sintering) porous ceramic substrates with zirconia dispersions, finding that repeated dipping led to a less porous coating, and to step-by-step crack repairing of the surface. Kozuka et al. (2000) studied the influence of the addition of polyvinylpyrrolidone (PVP) as a stress-relaxing agent in $BaTiO_3$ and lead zirconate titanate (PZT) films. Incorporated PVP in precursor for films, to be formed by single-step dip-coating, suppressed crack formation in PZT and $BaTiO_3$ coatings, and significantly decreased the tensile stress of $BaTiO_3$ films.

Chemical etching with HF of coated composites thermally treated at 1200 °C (Fig. 9c) revealed the presence of acicular crystallites of about 5 µm in SEM images, which can be indicative of mullite presence (Zhu et al., 2016).

XRD of the coated composite thermally treated at 1200 °C (Fig. 10) further corroborated the presence of mullite peaks as was found in XRD of powdered B-OHAl samples heated at the same temperature (Fig. 4b).

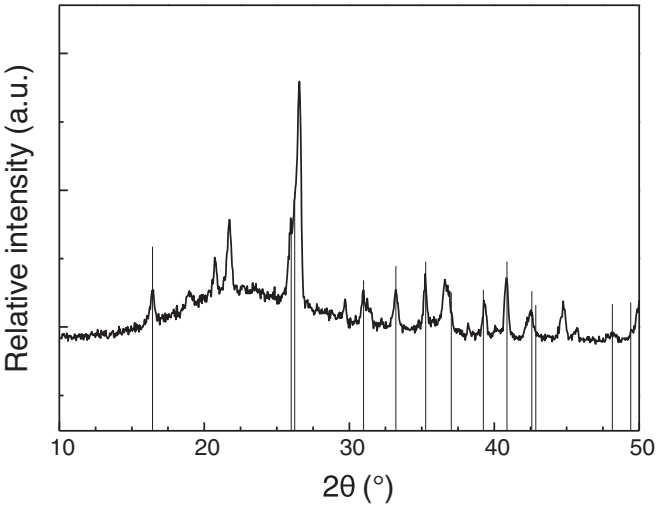

Fig. 10. XRD of Coated composite thermally treated at 1200 °C (mullite peaks marked below).

4. Conclusions

Polymeric Al-modified bentonite was found to be suitable as a precursor for mullite-containing coating on ceramic substrate. Rheological and electrokinetic properties of B-OHAl dispersions were tailored with the application of a polyacrylate based dispersant. Negative electrophoretic mobility of B-OHAl particles increased with NaPA adsorption. Well stabilized B-OHAl dispersion exhibiting newtonian flow behavior and low viscosity were prepared with a ratio of 2.8 NaPA/B-OHAl %g/g, which allowed its application in the dip coating process. Development of mullite, which is crystalline phase recognized for its good mechanical and thermal properties, and moderate densification of B-OHAl after heating at 1200 °C was observed. Coated composites were obtained by dipping porous substrates in stable and unstable B-OHAl dispersions and sintering at 1200 °C, in which the influence of the porosity of the substrate and the precursor dispersion on retained amount of coating and microstructure could be observed. Amount of coating significantly increased by immersing the more porous substrate in a stable dispersion. The presence of mullite in these coatings was corroborated by SEM.

Acknowledgments

The authors would like to thank CONICET and FONARSEC - NANOPETRO (Res. 454/12) for financial support.

References

Aceman, S., Lahav, N., Yariv, S., 2000. A thermo-XRD study of Al-pillared smectites differing in source of charge, obtained in dialyzed, non-dialyzed and washed systems. Appl. Clay Sci. 17, 99–126.

Alat, E., Motta, A.T., Comstock, R.J., Partezana, J.M., Wolfe, D.E., 2016. Multilayer (TiN, TiAlN) ceramic coatings for nuclear fuel cladding. J. Nucl. Mater. 478, 236–244.

Anggono, J., 2005. Mullite ceramics: its properties structure and synthesis. Jurnal Teknik Mesin 7, 1–10.

Aouad, A., Mandalia, T., Bergaya, F., 2005. A novel method of Al-pillared montmorillonite preparation for potential industrial up-scaling. Appl. Clay Sci. 28, 175–182.

Avena, M.J., Cabrol, R., De Pauli, C.P., 1990. Study of some physicochemical properties of pillared montmorillonites: acid-base potentiometric titrations and electrophoretic measurements. Clay Clay Miner. 38, 356–362.

Bernard, B., Bianchi, L., Malié, A., Joulia, A., Rémy, B., 2016. Columnar suspension plasma sprayed coating microstructural control for thermal barrier coating application. J. Eur. Ceram. Soc. 36, 1081–1089.

Bhattacharyya, K.G., Gupta, S.S., 2008. Adsorption of a few heavy metals on natural and modified kaolinite and montmorillonite: a review. Adv. Colloid Interf. Sci. 140, 114–131.

Bobzin, K., 2016. High-performance coatings for cutting tools. CIRP J. Manuf. Sci. Technol. http://dx.doi.org/10.1016/j.cirpj.2016.11.004.

Bottero, J., Bruant, M., Cases, J., 1988. Interactions between hydroxy-aluminium species and homoionic Na-and Ca-montmorillonite particles, as manifested by ζ potential, suspension stability and X-ray diffraction. Clay Miner. 23, 213–224.

Bouwmeester, H., Burgraaf, A., Burgraaf, A., Cot, L., 1996. Fundamentals of Inorganic Membrane Science and Technology. Elsevier, Amsterdam.

Brindley, G., Sempels, R., 1977. Preparation and properties of some hydroxy-aluminium beidellites. Clay Miner. 12, 229–237.

Choon Ong Ban, C., 2010. Surface Forces Arising from Polymers and Small Ionic Additives-Yield Stress and Zeta Potential Relationship. (Doctoral dissertation).

De León, M.A., De Los Santos, C., Latrónica, L., Cesio, A.M., Volzone, C., Castiglioni, J., Sergio, M., 2014. High catalytic activity at low temperature in oxidative dehydrogenation of propane with Cr–Al pillared clay. Chem. Eng. J. 241, 336–343.

Dietmar, V., Lengauer, C., Beran, A., Schneider, H., 2001. Infrared band assignment and structural refinement of Al-Si, Al-Ge, and Ga-Ge mullites. Eur. J. Mineral. 13 (3), 591–604.

Duval, D.J., Risbud, S.H., Shackelford, J.F., 2008. Mullite, Ceramic and Glass Materials. Springer, pp. 27–39.

Farmer, V.C., 1968. Infrared spectroscopy in clay mineral studies. Clay Miner. 7 (4), 373–387.

Gavin, P., Chevrier, V., Ninagawa, K., Gucsik, A., Hasegawa, S., 2013. Experimental investigation into the effects of meteoritic impacts on the spectral properties of phyllosilicates on Mars. J. Geophys. Res. Planets 118, 65–80.

Grim, R.E., K., G., 1961. Montmorillonite: high temperature reactions and classification. Am. Mineral. 46, 1329–1369.

Gu, Y., Meng, G., 1999. A model for ceramic membrane formation by dip-coating. J. Eur. Ceram. Soc. 19, 1961–1966.

Harsh, J.B., Doner, H., Fuerstenau, D., 1988. Electrophoretic mobility of hydroxy-aluminum and sodium-hectorite in aqueous solutions. Soil Sci. Soc. Am. J. 52, 1589–1592.

Jagota, S., Harmer, M.A., Lemon, M.F., Jagota, A., McCarron, E.M., 1995. Pillared smectite clay coatings for ceramic-matrix composites. J. Am. Ceram. Soc. 78, 2243–2247.

Kanda, Y., Iwamoto, H., Kobayashi, T., Uemichi, Y., Sugioka, M., 2009. Preparation of highly active alumina-pillared clay montmorillonite-supported platinum catalyst for hydrodesulfurization. Top. Catal. 52, 765–771.

Kloprogge, J., 1998. Synthesis of smectites and porous pillared clay catalysts: a review. J. Porous. Mater. 5, 5–41.

Kloprogge, J., Booy, E., Jansen, J., Geus, J., 1994. The effect of thermal treatment on the properties of hydroxy-Al and hydroxy-Ga pillared montmorillonite and beidellite. Clay Miner. 29, 153–167.

Kloprogge, J.T., Duong, L.V., Frost, R.L., 2005. A review of the synthesis and characterisation of pillared clays and related porous materials for cracking of vegetable oils to produce biofuels. Environ. Geol. 47, 967–981.

Kozuka, H., Kajimura, M., Hirano, T., Katayama, K., 2000. Crack-free, thick ceramic coating films via non-repetitive dip-coating using polyvinylpyrrolidone as stress-relaxing agent. J. Sol-Gel Sci. Technol. 19, 205–209.

Lagaly, G., 2006. Colloid Clay Science. Developments in Clay Science. 1. pp. 141–245.

Lee, W., Souza, G., McConville, C., Tarvornpanich, T., Iqbal, Y., 2008. Mullite formation in clays and clay-derived vitreous ceramics. J. Eur. Ceram. Soc. 28, 465–471.

Lee, J.-L., Kuo, K.-N., Sung, T.-L., Lai, Y.-T., 2016. Preparation of antibacterial ceramic coatings containing ag on titanium alloy by use of microarc oxidation. In: IEEE Transactions on Plasma Science. 44. pp. 3179–3182.

Liang, H.-N., Long, Z., Zhang, H., Yang, S.-H., 2010. Rheological properties of acid-activated bentonite dispersions. Clay Clay Miner. 58, 311–317.

Ma, L., Zhu, J., Xi, Y., Zhu, R., He, H., Liang, X., Ayoko, G.A., 2015. Simultaneous adsorption of Cd (ii) and phosphate on Al 13 pillared montmorillonite. RSC Adv. 5, 77227–77234.

Mackenzie, R.C., Caillère, S., 1979. Data Handbook for Clay Materials and Other Non-metallic Minerals. Pergamon Press.

Martinez, J.M., Volzone, C., Garrido, L.B., 2017. Thermal transformations up to 1200°C of Al-pillared montmorillonite precursors prepared by different OH–Al polymers. J. Therm. Anal. Calorim. 128, 61–69.

Mathieu, Y., Rigolet, S., Valtchev, V., Lebeau, B., 2008. Investigations of a sodium – Polyacrylate-containing system yielding Nanosized Boehmite particles. J. Phys. Chem. C 112, 18384–18392.

McConville, C.J., Lee, W.E., 2005. Microstructural development on firing illite and smectite clays compared with that in kaolinite. J. Am. Ceram. Soc. 88, 2267–2276.

Plee, D., Borg, F., Gatineau, L., Fripiat, J., 1985. High-resolution solid-state aluminum-27 and silicon-29 nuclear magnetic resonance study of pillared clays. J. Am. Chem. Soc. 107, 2362–2369.

Ramasamy, S., Tewari, S.N., Lee, K.N., Bhatt, R.T., Fox, D.S., 2011. Environmental durability of slurry based mullite–gadolinium silicate EBCs on silicon carbide. J. Eur. Ceram. Soc. 31, 1123–1130.

Santagata, M., Clarke, J.P., Bobet, A., Drnevich, V.P., El Mohtar, C.S., Huang, P.-T., Johnston, C.T., 2014. Rheology of concentrated bentonite dispersions treated with sodium pyrophosphate for application in mitigating earthquake-induced liquefaction. Appl. Clay Sci. 99, 24–34.

Schrijnemakers, A., Andre, S., Lumay, G., Vandewalle, N., Boschini, F., Cloots, R., Vertruyen, B., 2009. Mullite coatings on ceramic substrates: stabilisation of Al 2 O 3–SiO 2 suspensions for spray drying of composite granules suitable for reactive plasma spraying. J. Eur. Ceram. Soc. 29, 2169–2175.

Scriven, L., 1988. Physics and Applications of Dip Coating and Spin Coating, MRS Proceedings. Cambridge Univ Press, pp. 717.

Siffert, B., Espinasse, P., 1980. Adsorption of organic diacids and sodium polyacrylate onto montmorillonite. Clay Clay Miner. 28, 381.

Vaughan, D.E.W., Lussier, R., 1980. Preparation of molecular sieves based on pillared interlayered clays (PILC). In: Rees, L.V.C. (Ed.), Proc. 5th Inter. Conf. Zeolites. Heyden Press, London, pp. 94–101.

Vicente, M., Bañares-Muñoz, M., Gandía, L., Gil, A., 2001. On the structural changes of a saponite intercalated with various polycations upon thermal treatments. Appl. Catal. A Gen. 217, 191–204.

Vidal, N., Volzone, C., 2012. Influence of organobentonite structure on toluene adsorption from water solution. Mater. Res. 15, 944–953.

Volzone, C., Garrido, L.B., 2001. Retention of OH-Al complexes by dioctahedral smectites. Clay Miner. 36 (1), 115–123.

Volzone, C., Garrido, L.B., 2008. Use of modified hydroxy-aluminum bentonites for chromium (III) removal from solutions. J. Environ. Manag. 88, 1640–1648.

Volzone, C., Garrido, L.B., 2012. High temperature structural modifications of intercalated montmorillonite clay mineral with OH-Al polymers. Procedia Mater. Sci. 1, 164–171.

Wachtman, J.B., Cannon, W.R., Matthewson, M.J., 2009. Mechanical Properties of Ceramics. John Wiley & Sons.

Wang, K.-T., Cao, L.-Y., Huang, J.-F., Fei, J., Zhang, B.-Y., 2013. Microstructure and oxidation resistance of C-AlPO 4–mullite coating prepared by hydrothermal electrophoretic deposition for SiC C/C composites. Ceram. Int. 39, 1037–1044.

Wang, G., Zhang, S., Wang, J., Ma, S., Lu, X., Komarneni, S., 2016. Synthesis of porous Al pillared montmorillonite after pre-intercalation with dodecylamine: textural and thermal properties. J. Porous. Mater. 23, 1687–1694.

Xia, C., Zha, S., Yang, W., Peng, R., Peng, D., Meng, G., 2000. Preparation of yttria stabilized zirconia membranes on porous substrates by a dip-coating process. Solid State Ionics 133, 287–294.

Zhang, B., Huang, J., Ouyang, H., Cao, L., Li, C., 2016. A mullite oxidation protective coating on SiC coated carbon/carbon composites by hot dipping. Ceram. Int. 42, 17932–17935.

ZhongLiu, W., Peng, X., Zhuan, L., Wen, H., Heng, L., XiaoYu, Y., Yang, L., WenBo, C., 2015. Microstructure and oxidation behavior of sol–gel mullite coating on SiC-coated carbon/carbon composites. J. Eur. Ceram. Soc. 35, 3789–3796.

Zhu, Z., Wei, Z., Sun, W., Hou, J., He, B., Dong, Y., 2016. Cost-effective utilization of mineral-based raw materials for preparation of porous mullite ceramic membranes via in-situ reaction method. Appl. Clay Sci. 120, 135–141.